A&A 380, 504–515 (2001)
DOI: 10.1051/0004-6361:20011434

Astronomy & Astrophysics

The new cataclysmic variable RX J1554.2+2721 in the period gap

G. H. Tovmassian[1], J. Greiner[2], S. V. Zharikov[1], J. Echevarría[3], and A. Kniazev[4]

[1] Observatorio Astronómico Nacional*, Instituto de Astronomía, UNAM, Ensenada, B.C., México
[2] Astrophysical Institute Potsdam, An der Sternwarte 16, 14482 Potsdam, Germany
[3] Instituto de Astronomía, UNAM, Apartado Postal 70-264, 04510 México, D.F., México
[4] Special Astrophysical Observatory of RAS, Nizhnij Arkhyz, 357147, Russia

Received 12 July 2001 / Accepted 24 September 2001

Abstract. We report on the results of a spectroscopic and photometric study of a new cataclysmic variable, identified as optical counterpart of the X-ray source RX J1554.2+2721 detected by ROSAT. The spectroscopic observations of the relatively bright ($\sim 16\overset{\mathrm{m}}{.}5$) object show systematic radial velocity variations with a semi-amplitude of $\sim$140 km s^{-1}. Besides the clear presence of distinct low and high states there are periodic photometric light variations with an amplitude of about 0.15 mag in the R band. The orbital period is $2\overset{\mathrm{h}}{.}753$ thus being within the period gap, at its upper border. The flux distribution in the spectrum of the object shows a substantial contribution of a M4 V secondary, and also bears clear signs of cyclotron emission. Thus, we classify the discovered object as a new member of the AM Her class of magnetic cataclysmic variables. This classification is further supported by the soft X-ray spectrum, the characteristic profiles of the emission lines, the tomography map and the shape of the orbital light curve. A simple fitting of the spectrum in the low and high states suggests a reduced mass transfer rate in RX J1554.2+2721 compared to similar objects outside the period gap.

Key words. stars: individual: RX J1554.2+2721 – stars: novae, cataclysmic variables – stars: binaries: close – X-rays: stars

1. Introduction

Cataclysmic variables (CVs) are close binary systems in which mass is transferred from a red dwarf star that fills its Roche lobe onto a white dwarf (WD). The AM Her stars, or polars, are a subclass of CVs containing a synchronously rotating, accreting, magnetic white dwarf. The high ($B \geq 5$ MG) magnetic field of the WD prevents the formation of an accretion disc and channels the transferred matter along the magnetic lines directly onto the surface of the WD (Warner 1995). The polars, in contrast to many other CVs accreting through a disk, do not produce dwarf nova outbursts, but rather switch erratically from high luminosity states to low states. These changes in luminosity are believed to be due to a change in mass transfer rate. The reason for such changes is not clear, although irradiation of the secondaries in polars might be one of the contributing factors (King & Cannizzo 1998). Alternative possibilities and an extensive discussion of such behavior in polars has been presented by Howell et al. (2000).

As a rule, the orbital period of a CV is a precisely known physical parameter. Usually, CVs have orbital periods ranging from 80 min up to ∼10 hours with a highly significant deficiency (called the *orbital period gap*) at $2^{\mathrm{h}} < P_{\mathrm{orb}} < 3^{\mathrm{h}}$ (e.g., Robinson et al. 1983; Ritter et al. 1995). Over the past decade, only ∼25 CV systems were reported to have periods between $2\overset{\mathrm{h}}{.}0$ and $3\overset{\mathrm{h}}{.}0$ among ∼300 CVs with known orbital periods (Downes et al. 1997). The existence of the period gap is most commonly explained in terms of angular momentum loss during evolution. Magnetic breaking is considered the driving force for the systems above the period gap (Rappaport et al. 1983). It halts at the periods of ≈3 hours. Then the systems drift to smaller separations without mass transfer and thus are faint and mostly unobservable as a CV. At periods of about 2 hours, other mechanisms, e.g. gravitational waves, become significant to ignite the mass flow from the donor star, and the system regains its brightness because accretion resumes (Howell et al. 1997 and references therein). However, polars are found rather often in the period gap, either narrowing it substantially or casting doubt on its existence at all. The observed low value of the mass transfer rate for polars is sufficient

Send offprint requests to: G. H. Tovmassian,
e-mail: gag@astrosen.unam.mx
* Use for smail PO Box 439027, San Diego, CA, 92143-9027, USA.

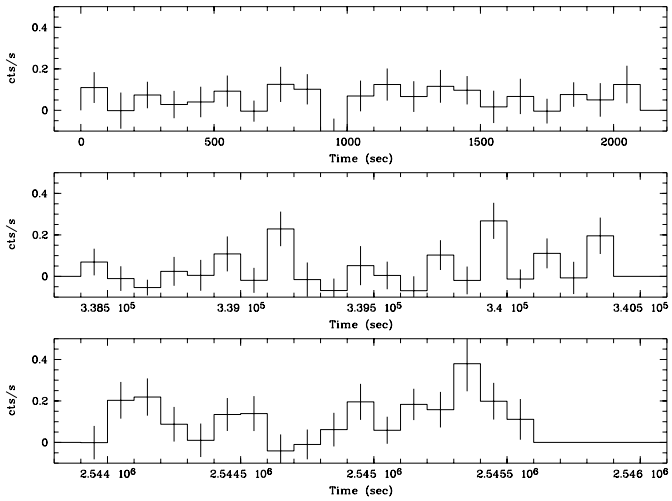

Fig. 1. X-ray light curve of RX J1554.2+2721 derived from the pointed ROSAT PSPC observation 800551p in Jul./Aug. 1993. The observation was split into three observation intervals, separated by 3.9 and 25 days, respectively. Each of the panels shows a 2300 s stretch of the observation with the time given relative to the start of the observation.

reason for the absence of a period gap in their distribution (Wickramasinghe & Wu 1994). As Li et al. (1994) have shown, the magnetic breaking may not apply to magnetic systems.

Here we report the discovery of a new cataclysmic variable, called RX J1554.2+2721 (=1RXS J155412.7+272143) which is of the AM Her type (the ROSAT source was very recently identified independently as a CV by Jiang et al. (2000), while this paper was in preparation). RX J1554.2+2721 has an orbital period of $2\overset{\mathrm{h}}{.}753$, which places it at the very edge of the upper limit of the period gap. Each new object in the period gap is very important for theoretical models of the evolution of CVs.

2. Observation and data analysis

2.1. X-ray observations

RX J1554.2+2721 was scanned during the ROSAT all-sky-survey over a period of 4 days in August 1991 for a total observing time of 380 s. Its mean count rate in the ROSAT position-sensitive proportional counter (PSPC) was 0.12 cts/s, and the hardness ratio $HR1 = -0.78 \pm 0.15$ where $HR1$ is defined as $(H-S)/(H+S)$, with $H(S)$ being the counts above (below) 0.4 keV over the full PSPC range of 0.1–2.4 keV.

RX J1554.2+2721 was serendipitously covered by a pointed ROSAT PSPC observation, though at very large off-axis angle. This observation (800551p) was performed in July/August 1993 for 6090 s, and detects RX J1554.2+2721 at a (vignetting corrected) mean count rate of 0.14 cts/s. For the spectral and timing analysis the source photons were extracted with a radius of $6\overset{'}{.}5$. The background was chosen between 7.5–10′ wide ring sector of 270° disregarding a 90° part along the rim of the field of view. Standard corrections were applied using the dedicated EXSAS software package (Zimmermann et al. 1994).

2.1.1. X-ray light curve

The light curve of the three separate exposure intervals of observation 800551p in July/August 1993 is shown in Fig. 1 with a 100 s binning. Two things are immediately obvious: (i) the count rate varies between a mean floor of 0.1–0.2 cts/s to up to 0.4 cts/s during peaks; and (ii) there are "dips" of nearly zero count rate at regular intervals of about 400 s. These "dips" are due to the wobble of the ROSAT satellite which occasionally places RX J1554.2+2721 outside of the field-of-view. Thus, the mean count rate as given above is certainly a lower limit to the actual intensity. Apart from this cosmetic effect, this also makes a folding over the best-fit orbital period (see below) useless, since it introduces spurious features in addition to the low phase coverage caused by the short exposure time.

2.1.2. X-ray spectrum

The X-ray spectrum during the pointed observation is very soft ($HR1 = -0.9 \pm 0.1$). Fitting a one-component model, e.g. a simple black body model, results in a large reduced $\chi^2 = 2.8$. Applying a sum of a black body and a thermal bremsstrahlung model with the temperature of the latter component fixed to 20 keV (it is not constrained at all by the ROSAT data) gives a good reduced $\chi^2 = 0.9$ (see Fig. 2) and the following fit parameters: $kT_{\rm bbdy} = 17 \pm 15$ eV, $N_{\rm H} = 3.3 \times 10^{20}$ cm^{-2}. For a better comparison to the parameters of similar sources we also fixed the black body temperature to $kT_{\rm bbdy} = 25$ eV, and derive $N_{\rm H} = 1.5 \times 10^{20}$ cm^{-2}, $\mathrm{Norm}_{\rm bbdy} = 0.045$ and $\mathrm{Norm}_{\rm thbr} = 2.6 \times 10^{-5}$. This gives an unabsorbed 0.1–2.4 keV flux of 2×10^{-12} erg cm^{-2} s^{-1} (or 5×10^{-12} erg cm^{-2} s^{-1} bolometric), corresponding to an unabsorbed bolometric luminosity of 6×10^{30} $(D/100\ \mathrm{pc})^2$ erg s^{-1}.

2.2. Optical observations

The CCD photometric and spectroscopic observations of RX J1554.2+2721 were carried out at the 1.5 m and 2.12 m telescopes of the Observatorio Astronómico Nacional de San Pedro Mártir (OAN SPM), Mexico and at the 6 m telescope of the Special Astrophysical Observatory of the Russian Academy of Sciences (SAO RAS). The log of observations is presented in the Table 1. Inspection of the spectrum of the brightest object in the ROSAT 30″ error box (Fig. 3) showed that it has spectral characteristics typical to a CV. The USNO catalog gives the following measurements: U1125 07424531: $15^{\rm h}54^{\rm m}12\overset{''}{.}40 + 27°21'51\overset{''}{.}2$, $R = 16\overset{\rm m}{.}5$ and $B = 15\overset{\rm m}{.}9$ for this object.

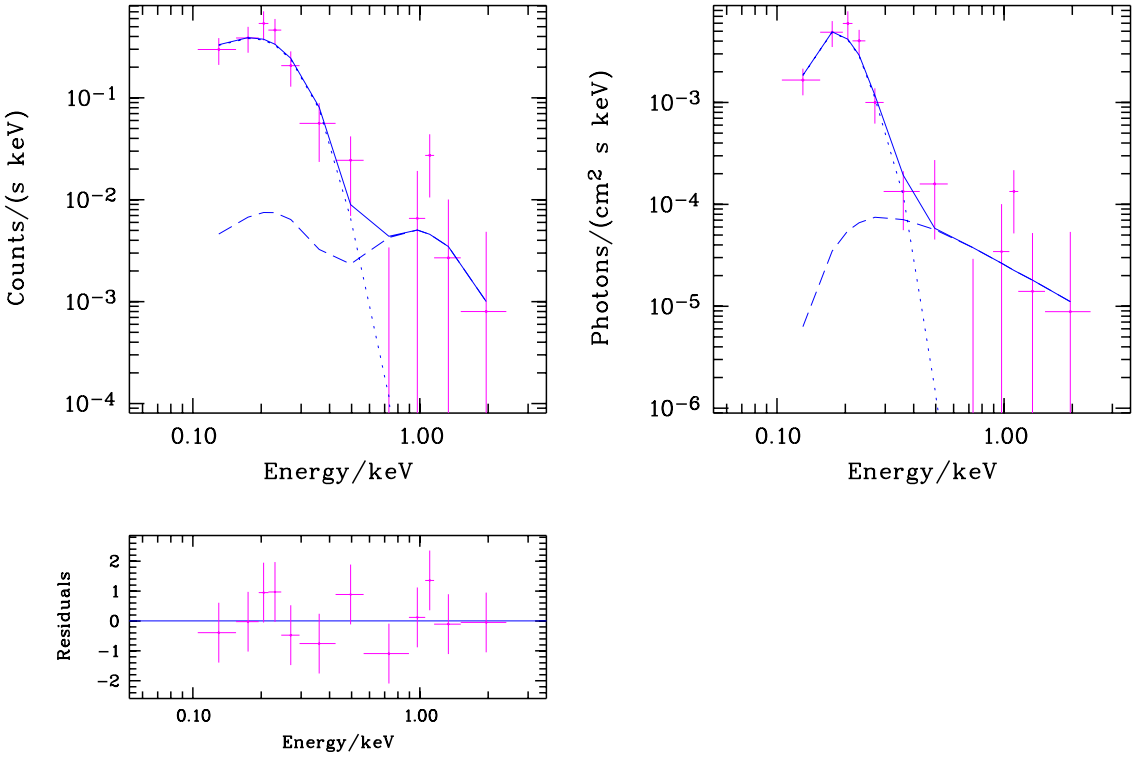

Fig. 2. ROSAT PSPC X-ray spectrum of RX J1554.2+2721 derived from the pointed observation 800551p fitted with a sum of a blackbody and a thermal bremsstrahlung model. The lower left panel shows the deviation between data and model in units of χ^2 per bin.

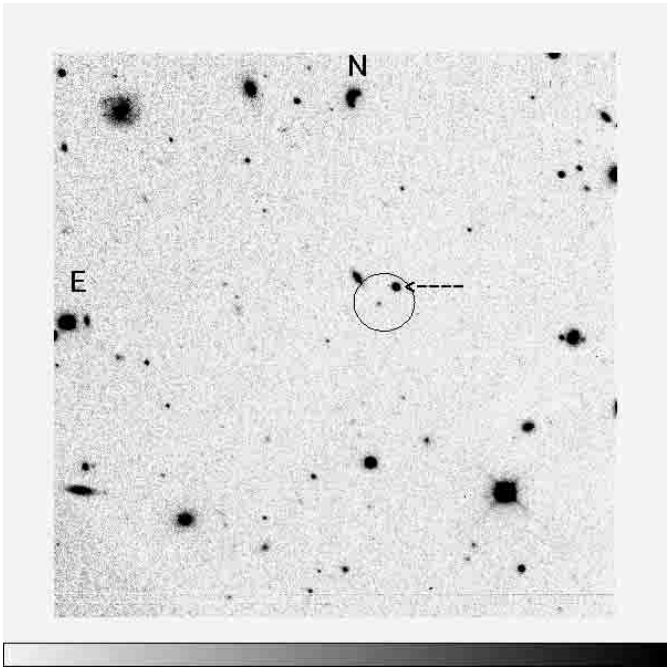

Fig. 3. Identification chart showing the field of RX J1554.2+2721. The circle in the center shows the ROSAT 30″ error box.

An identification chart of RX J1554.2+2721 is given in Fig. 3 with the CV marked.

2.2.1. Optical photometry

We obtained time-resolved R_c-band photometry of RX J1554.2+2721 during two nights on May 26 and August 1st, 2000 at the 1.5 m telescope. Several additional measurements were obtained in March and October 2000. The telescope was equipped with a SITE CCD in a direct imaging mode. In total, the object was monitored during $\sim 6\overset{h}{.}3$ ($3\overset{h}{.}3$ the first night and 3^h the second night). The exposure times were 300 s and 180 s, respectively, which leads to a time resolution of 350 and 230 s, taking into account the dead time due to read-outs. The standard reduction techniques of CCD photometry were applied using the DAOPHOT package in IRAF to measure differential magnitudes. The images were corrected for bias and flat-field before aperture photometry was carried out. The dispersion of magnitudes ranged from 0.005 to 0.01 mag as measured from the differential photometry of comparison stars with a similar brightness. Unfortunately, no absolute calibration for our photometric data was obtained.

The light curve shows $\approx 0\overset{m}{.}15$ smooth brightness variations. The nightly mean magnitudes fall into two categories, with 0.6 mag difference between them. The shape of the light curves changes together with the change of the mean magnitude. There is no notable flickering or short time scale oscillations. For the results of the period analysis and the differences in the light curves as well as their interpretation we refer to the following sections.

Table 1. Log of optical observations.

Date (2000 year)	HJD start 2541000+	Duration (min)	Exposures (s)	Band/Wavelength	Telescope/Equipment
16 Mar.	619.82	118	300	R_c	1.5 m CCD
11 Apr.	646.002	20	600	3680–7580	2.12 m B&Ch spectrograph
12 Apr.	647.901	167	600	3450–5100	2.12 m B&Ch spectrograph
26 May	691.748	200	300	R_c	1.5 m CCD
1 Aug.	758.518	180	180	R_c	1.5 m CCD
18 Sep.	805.637	83	720	3550–5530	2.12 m B&Ch spectrograph
05 Oct.	822.613	83	720	3680–5650	2.12 m B&Ch spectrograph
06 Oct.	823.65	30	600	3660–8100	6 m UAGS
06 Oct.	823.60	10	600	R_c	1.5 m CCD

2.2.2. Optical spectrophotometry

Two spectra of the object were taken on April 11, 2000 using the Boller & Chivens spectrograph installed in the Cassegrain focus of the 2.12 m telescope of OAN SPM. The 300 l/mm grating was used to cover a wide range of wavelengths spanning from 4000 to 7600 Å.

Time-resolved spectroscopy of the optical counterpart of RX J1554.2+2721 was obtained on April 12 and September 18, 2000 on the same telescope and same spectrograph. We used the 400 l/mm grating with a 13°54 blaze in the second order, combined with the blue BG39 filter and a TEK1024 × 1024 pixel CCD with a 0.24 μ pixel size. The slit width was 1.5 arcsec projected on the sky. The seeing was satisfactory with ≤1.2 arcsec. The exposure times were 600 and 720 s. The spectral range from λ 3800 Å to 5100 Å was covered with spectral resolution of 1.5 Å/pix leading to a 2.8 Å *FWHM* resolution. In total, 26 spectra were obtained, among them eight in September 2000.

A number of additional spectra were obtained in October 2000. Two spectra were obtained on October 5 with similar settings as the previous September observations at SPM. During the next night we acquired three more spectra with the 6 m telescope of SAO in Russia, one in the blue region λ 3700–6100 Å and two at λ 5700–8100 Å wavelength range. The UAGS spectrograph with the Photometrix CCD was used in order to obtain ≈5 Å *FWHM* resolution spectra. He-Ar arc spectra were used during all observations for wavelength calibration. In all cases except the September and October SPM observations, spectrophotometric standard stars were observed in order to perform flux calibration. The IRAF long slit spectroscopic reduction package was used for the extraction of spectra, wavelength and flux calibrations. Before these steps, the images were corrected for bias and cosmic rays.

It appeared that the October spectra were obtained when RX J1554.2+2721 was in a low state, while the rest of the spectra were acquired with the system being in a high state.

In Fig. 4 we present the average (after correcting the wavelengths for orbital motion) of all high-resolution spectra and the red portion of the low-resolution spectra of RX J1554.2+2721 in the high state. They exhibit all emission lines characteristic of CVs, and also clear TiO absorption features from the M-dwarf secondary. Some major spectral features are marked in Fig. 4. A comparison with spectra of main-sequence late type stars yields a spectral type later than M3 V and earlier than M5 V. A M4 V spectrum is also presented in Fig. 4. There is a small deficiency in flux at λ 7300–7600 Å, between the object and the standard, which may indicate a slightly later type ≈M4.5 V. We subtracted the standard M4 V star spectrum from the sum of low-resolution spectra of RX J1554.2+2721. The resulting spectrum is shown in the lower panel of Fig. 4.

3. Orbital period

The bright Hβ line was deblended with two Gaussians as a first step, common for such kind of objects (Schwope et al. 1997; Tovmassian et al. 1999). The resulting components fall into two categories according to their widths, amplitudes of radial velocity (RV) variations and phases. The dominant and thus more easily distinguishable narrow emission line (NEL) component shows a *FWHM* of approximately 4–6 Å. It was separated from the rest, and underwent period analysis. The power spectrum produces a broad peak around 8.7 day^{-1} if only the data of one night with the longest coverage are used. The corresponding power spectrum is presented in the lower panel of Fig. 5. Its maximum value closely coincides with the photometric period. The photometric data also produce a broad feature in the power spectrum (second panel from the bottom in Fig. 5). Adding the September data to the spectroscopic sequence moves the highest peak in the power spectrum to shorter periods (third panel). Finally, including two more points obtained in October, shifts the highest peak in the power spectrum to a higher frequency (≈9.7 day^{-1}), as can be seen on the top panel of Fig. 5. However, the latter value hardly can be acceptable, since the analysis of one night data does not support the possibility of such short a period. We selected the maximum peak in the range of values between 8.5 and 9.0 day^{-1} as the most plausible for the orbital period of RX J1554.2+2721. This corresponds to $0\overset{\mathrm{d}}{.}11473 \pm 0\overset{\mathrm{d}}{.}0006 = 2\overset{\mathrm{h}}{.}7535$. This error of period estimation is rather technical, assuming that we selected the right peak in the power spectrum. However, we do

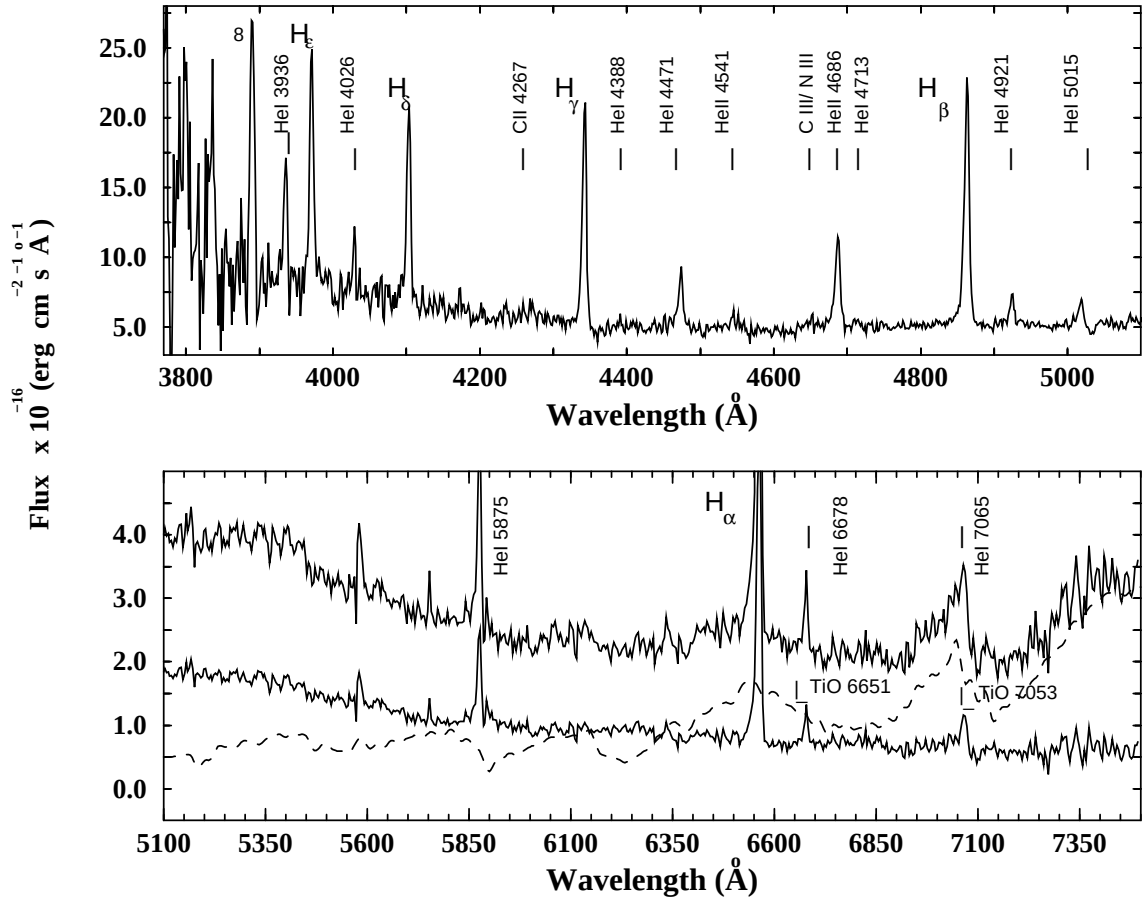

Fig. 4. The sum of high state spectra of RX J1554.2+2721 obtained in April 2000. The upper panel shows higher resolution spectra in the blue part. In the bottom panel red portion of lower resolution spectra is presented. Most of the spectral lines are marked. The spectrum of the M4 V standard star and the result of subtraction of the red star from the observed spectrum of RX J1554.2+2721 are presented.

not have an efficient way to unambiguously distinguish it based on our data. *(When this paper was already submitted for publication, Thorstensen et al. (2001) reported a* $2\overset{\mathrm{h}}{.}52$ *period for this object, which does not contradict our period analysis, nor the main results following from there.)*

Assuming that the NEL component originates from the heated front portion of the secondary star (as it is common in a number of AM Her systems, e.g. Schwope et al. 1997; Tovmassian et al. 1999), the radial velocity curve derived from the NEL measurements was fitted with a sine curve with the derived orbital period of $P_{\rm orb} = 0.11473$ days:

$$v(t) = \gamma_0 + K_2 * \sin(2\pi(t - t_0)/P), \quad (1)$$

where γ_0 is the systemic velocity, and K_2 is the semi-amplitude of the radial velocity of the secondary star, both in $\mathrm{km\,s^{-1}}$. The observation time is t, the epoch $t_0 = 2451761\overset{\mathrm{d}}{.}2281 \pm 0\overset{\mathrm{d}}{.}0001$ corresponds to the −/+ zero crossing of the Hβ radial velocity curve, and therefore the inferior conjunction of the secondary star. Our best fit yielded $K_{\rm NEL} = 139\ \mathrm{km\,s^{-1}}$ with a standard deviation of $\sigma = 43\ \mathrm{km\,s^{-1}}$. The RV curve and our fit of the NEL component are presented in the bottom panel of Fig. 6.

The other component, although not well distinguished at some phases, has an amplitude and orbital phasing typical for the high velocity component (HVC) as defined in studies of magnetic CVs (Cropper 1990; Schwope et al. 1997). It is assumed to originate in the ballistic part of the accretion stream. The HV component of emission lines is shown on the upper panel of Fig. 6. The fit of the radial velocities from the NEL is over-plotted for comparison.

4. The system composition: High and low states

4.1. Photometry

As mentioned above, the system switches from one luminosity state to the other very frequently. We present the behavior of the object in Fig. 7. The mean differential magnitudes of the system in comparison to a nearby star as measured from photometric observations differ by up to $0\overset{\mathrm{m}}{.}65$. In the case of spectral observations, when no flux calibration was available, we can guess the state of the system from the appearance of the spectrum. It shows that the system undergoes a change of state almost every month. Actually, we do not know any other similar system in which these state changes so frequently.

Figure 8 demonstrates the $R_{\rm c}$ light curve of RX J1554.2+2721 folded with the orbital period and

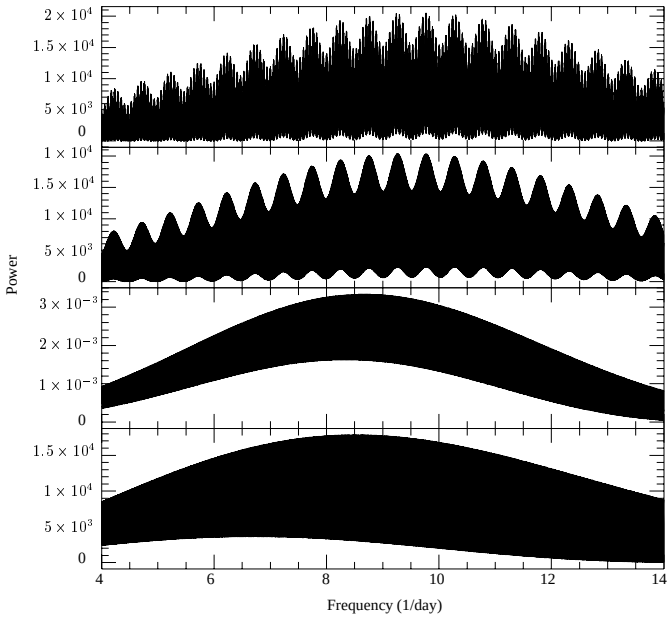

Fig. 5. The power spectra of RX J1554.2+2721 obtained from analysis of: (from bottom to top) first panel: Hβ NEL radial velocities from April observations; second panel: two nights of R band photometry; third panel: Hβ RV data with addition of September data; forth panel: same as in third panel with addition of October points.

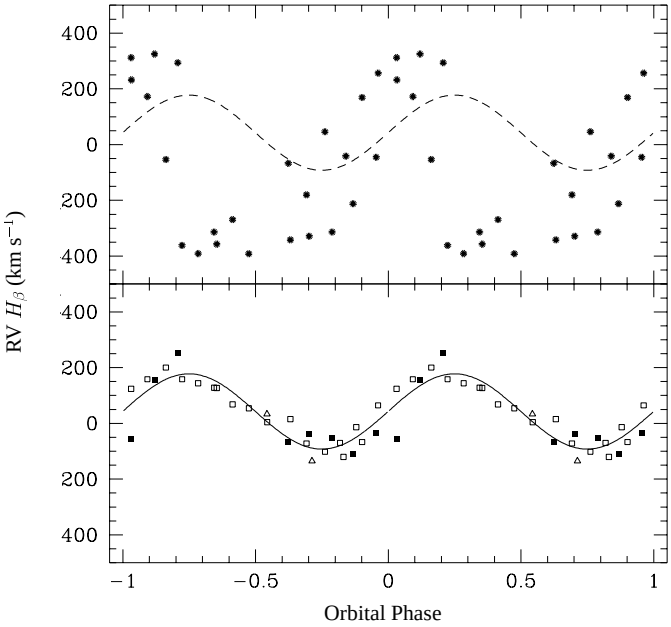

Fig. 6. The radial velocity curves or the NEL and HV component of the Hβ emission line on the bottom and upper panels, respectively. The solid line is a *sin* fit to the NEL radial velocities repeated on both panels for comparison. The open squares mark observations of April, black squares are those from September and open triangles mark October measurements. Asterisks in the upper panel represent the HVC poorly determined measurements.

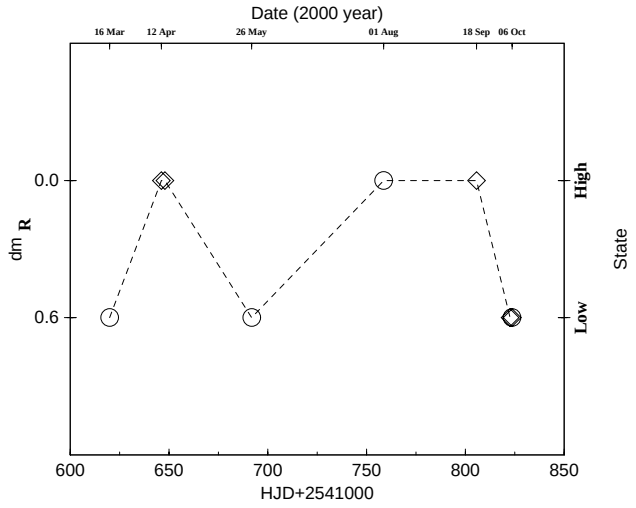

Fig. 7. The behavior of the system during the period of our observations. The circles are differential magnitudes determined from photometry. The left vertical axes display differential magnitudes in comparison to the field stars. The diamonds mark spectroscopic determination of the luminosity state and its height is symbolic marked on the right vertical axes

phased according to the above-derived orbital parameters. The bottom panel displays the light curve obtained in the low luminosity state. The upper panel presents the light curve of RX J1554.2+2721 while the system was in the high state. There are several important features which distinguish these two curves:

In the low state the system shows a pronounced double humped curve. Taking into account the large contribution of the secondary in the total light we assume that in the R band during the low state we see mainly the surface of the secondary star. It is elliptically distorted by filling its corresponding Roche lobe and irradiated. This causes the double hump feature with uneven depth of the minima. This is due to the changing aspect of the secondary's Roche-lobe which presents the largest projected area, and hence highest flux at phases 0.25 and 0.75. At phase 0.0 and 0.5 the projected area is the smallest. The flux decrease at phase 0.5 is smaller than at phase 0.0, because that side of the secondary has a higher temperature due to illumination, and hence is more luminous than the back side.

We estimate the mean amplitude of brightness variation from our R_c band light curve to be 0.13 mag in the low state. Using the equation (2.109b) from Warner (1995) we obtain an inclination of the system of 45°–55°, assuming a mass ratio $0.42 < q < 0.62$ for corresponding masses of the white dwarf of 0.39−0.57 $M_\odot$ and secondary mass of M4 $v = 0.24$ $M_\odot$ (Schmidt-Kaler 1982). The equation is very sensitive to a number of parameters. We were able to confirm and select a plausible solution q–i by means of Doppler tomography (see below).

The light curve in the high luminosity state is similar, but the double hump feature is smeared out by some additional emission. The amplitude of variation is about 0.2 magnitudes, a $\sim 0\overset{m}{.}07$ increase from the low state value. The primary minimum is also changed, being broader and flatter at the bottom. We suppose that additional

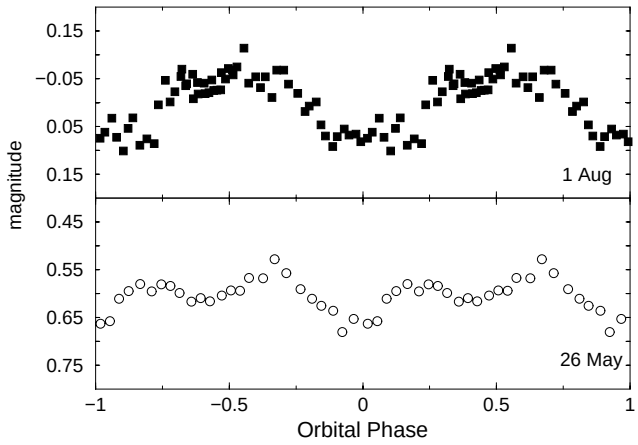

Fig. 8. Phase folded R_c light curves of RX J1554.2+2721, separately in high state (upper panel) and low state (bottom panel).

cyclotron emission starts to play a role in the total flux, when the pole is in view. There is also a significant contribution of the Hα line in the high state in comparison to the low state. Also, there appears to be some flickering in the light curve during the high state.

4.2. Spectrophotometry

The changes in the spectra of RX J1554.2+2721 between the high and low states are even more drastic. The broad band photometry in R includes a large contribution from the secondary, while the change of flux is conditioned by the accretion rate, and thus significant changes occur in the blue part of the spectrum. In Fig. 10 the low resolution spectra of RX J1554.2+2721 are presented in both states. The red portion of the spectra are dominated by the secondary star. It is very unusual that any cataclysmic variable in a high state, with a period shorter than 4–6 hours, will bear clear signs of its secondary in its spectrum at wavelengths shortward of Hα. Commonly, the contribution from accretion, either disk in most CVs or magnetic driven in polars, is the dominating source of light in the whole optical range during the high state. Therefore, we conclude that in RX J1554.2+2721 we have a reduced accretion rate even during the high state.

Another indication of low accretion is the narrowness of the emission lines of the system when it is in the low state. Actually, their regular Gaussian profiles, the 4 Å full widths as measured in two higher resolution spectra obtained in October, and the absence of the high velocity component belonging to the accretion stream suggests an almost complete halt of the mass transfer.

The blue part of the continuum completely changes its shape when the system switches from the high to the low luminosity state. The humps seen in the continuum during the high state become more pronounced, and the blue end of the spectrum drops by up to one order of magnitude. In order to understand the composition of the system, we have to examine the major contributors of emission in polars. In polars, except for photospheric emission from both components (which can be readily excluded here), the widely accepted sources of the flux are the following four components originating in the hot postshock region or its vicinity, where in-falling matter above the magnetic pole slows down and heats up before settling on the surface of the WD:

- Hard X-ray bremsstahlung emitted from an optically thin column;
- Blackbody radiation, thermalized and remitted by the heated surface of the WD in the soft X-ray and UV regions;
- Cyclotron emission from the column. It is emitted in a wide range of wavelengths from the near UV to the infrared region;
- Recombination emission, depending on the strength of the illuminating X-rays.

We are primarily interested in the latter two as the most probable sources of light in the blue part of our spectra.

4.3. Continuum modelling

Examination of the spectral appearance in the low state, where cyclotron lines are seen as broad humps in the continuum, and comparison to identical objects (most remarkably HS 1023+3900, Reimers 1999), strongly advocate the cyclotron nature of the observed flux. Actually, if not for the slight emission remaining in the lower order Balmer lines, apparently coming from the irradiated secondary, and significant contribution of the secondary photosphere in the continuum, the spectrum of RX J1554.2+2721 in the low state is very similar to that of HS 1023+3900 during its low state. The difference is only in the location of the cyclotron humps due to the difference in magnetic field. Luckily, in the case of RX J1554.2+2721 we have observed the system spectroscopically in both luminosity states, high and low. In the high state, the spectral appearance is notably different. We can see broader, multicomponent emission lines, higher orders of Balmer lines and appearance of not very strong He II emission in the spectrum, completely absent in the low state. In addition, a hot component changes the slope of the continuum in the blue side of the spectrum. We subtracted the low state spectrum from the averaged spectrum in the high state. The absence of orbital coverage in the low state prevents us from studying phase related effects. The resulting energy distribution, presented in Fig. 9, clearly consists of two components. Redward of 4800 Å it is flat, while blueward it rises steeply (power law index = −4!). It can hardly be attributed to the blending by Balmer lines in the vicinity of the Balmer jump (the Balmer lines are well resolved in the higher resolution spectra up to H_{10}, yet continuum is consistent with the lower resolution spectra), nor to the simple addition of a black body, e.g. from a hot spot. The power law is presented by the dashed line in Fig. 9, it roughly indicates a blackbody with $T_{\rm eff} \gg 100\,000$ K.

As an alternative to cyclotron emission, the low and high state transition could potentially also be due to off/on states of recombination emission. In the low state there is no He II emission at all, and He I is very weak, indicating that the excitation by X-rays is very low. Thus, it is conceivable that the illumination of the stream is so low that also no recombination emission is present. If, during the optical high state, the accretion rate increases, X-ray emission sets in, causing accordingly He II excitation, and also recombination emission. Normally in magnetic CVs one would expect recombination emission to come from a stream where typical assumed temperatures are of the order of only 20 000 K. We calculated the recombination emission energy distribution for 20 000 K and also for hypothetical source with temperatures as high as 5 and 15 keV. The input parameters are the edge energy (Paschen jump in our case), the temperature and a normalization parameter. The dot–dashed line in the Fig. 9 corresponds to a 15 keV temperature. Lower temperature curves are naturally much flatter. Even a 15 keV source is apparently not steep enough to satisfactorily fit the additional source of emission. The slope actually does not depend on the temperature of the source, thus recombination emission solely cannot be responsible for explaining the transformation.

We sought an explanation for the continuum energy distribution of RX J1554.2+2721 and its changes in cyclotron emission, and found satisfactory fits to explain both high and low luminosity states. The solution is not commonly applicable to other polars, but we consider this object to be of a different breed along with HS 1023+3900 due to its very low accretion rate, distinct from polars outside the "period gap". There is an extensive theoretical work on modelling the transfer of radiation through the standard accretion column (Chanmugam 1981; Meggitt & Wickramasinghe 1984; Barrett & Chanmugam 1984). Barrett & Chanmugam (1985) applied their models to fit the spectra of the magnetic CV VV Pup. We followed their procedures in constraining our models in order to describe the observed flux of RX J1554.2+2721. The authors demonstrate how the absorption and emission features of cyclotron emission originate and how they differ. In order to obtain an absorption spectrum one has to assume the presence of a cooler magnetized plasma layer with a hotter blackbody (BB) source behind it, representing the postshock region. On the other hand, an emission cyclotron spectrum will arise from the slab of plasma representing the postshock region of the accretion column itself. The comparison of sample models presented by Barrett & Chanmugam (1985), demonstrates that in the case of a pure emission spectrum the blue end of the spectrum is rapidly decreasing. At the same time, the absorption cyclotron spectrum, from an optically thick slab, is Rayleigh-Jeans-like and exhibits a steep rise toward the blue, similar to blackbody radiation.

Regarding the modelling, it is necessary to note that the absorption cyclotron spectrum was never used in the actual modelling of any observed object, even by the

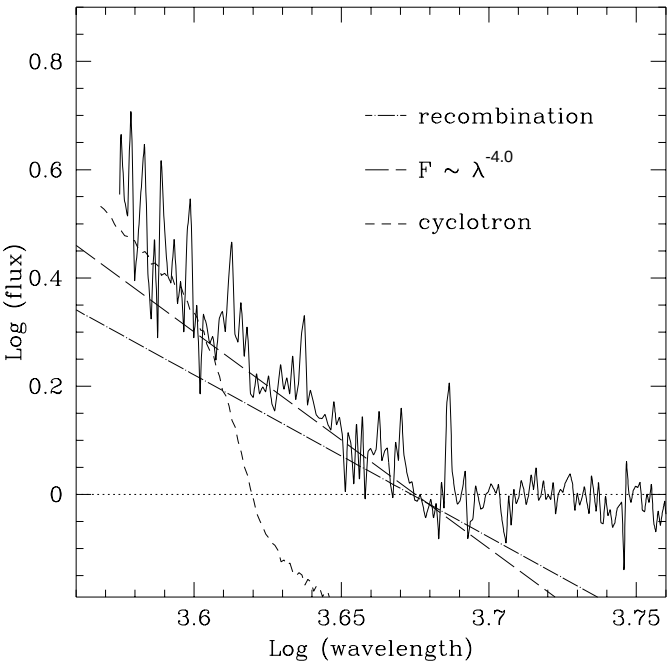

Fig. 9. The differential spectrum of RX J1554.2+2721 between high and low luminosity states. The additional emission responsible for changes is very "hot". The dashed line representing a power law is drawn to give an idea of its steepness. Also plotted are flux distributions of recombination emission and cyclotron optically thick emission.

authors of the model. The abovementioned model does not take into account the geometry of the magnetic spot, while there are modern models (e.g Woelk & Beuermann 1992; Rousseau et al. 1996 and more recently Fischer & Beuermann 2001), that successfully calculate corresponding parameters over the whole white dwarf atmosphere. However, on the one hand being restricted by a few spectra in the low state not covering all orbital phases, and on the other hand being able to achieve satisfactory results in fitting the observed flux distribution by simple models, we did not aim to determine the exact parameters of the system by applying state of the art models, rather, we have sought an explanation of its nature.

Thus, we used the Barrett & Chanmugam (1985) model to fit the observed continuum of RX J1554.2+2721 by a least square fit of

$$\sigma = \sqrt{\sum_{\lambda} (F_{\rm obs}(\lambda) - F_{\rm mod}(\lambda))^2} \qquad (2)$$

where $F_{\rm obs}$ are relative fluxes normalized to $F_{\lambda 8100} = 1$ in the low or high state with emission lines excluded from the analysis. $F_{\rm mod}$ is actually a sum

$$F_{\rm mod} = a * F_{\rm em} + b * F_{\rm M4} + c * F_{\rm abs}, \qquad (3)$$

where $F_{\rm em}$ is cyclotron emission from an optically thin medium, while $F_{\rm abs}$ is cyclotron emission from optically thick parts of the accretion column, and $F_{\rm M4}$ is the spectrum of the M4 V secondary star. The coefficients a, b

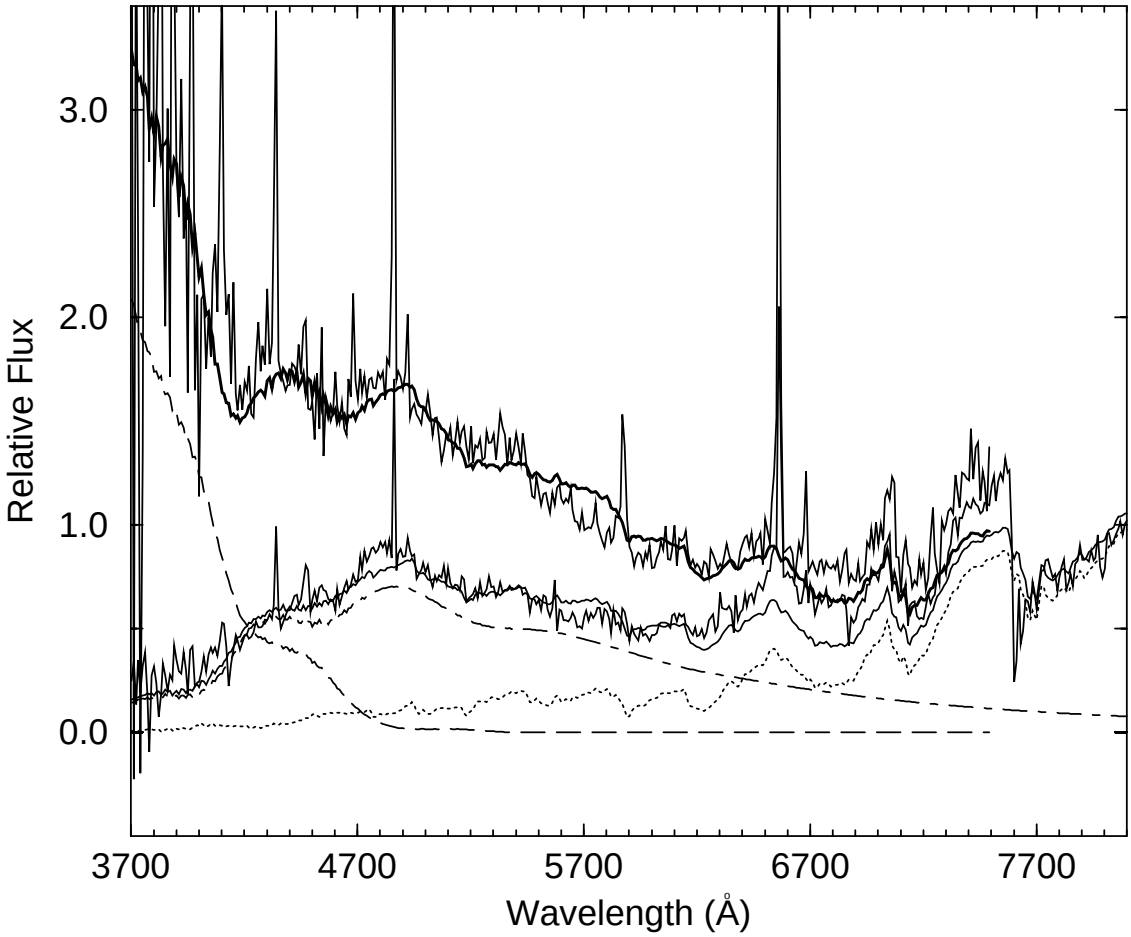

Fig. 10. The low-resolution spectra of RX J1554.2+2721 in high and low states are presented (thin solid line). The dotted line corresponds to the M4 v star spectrum. Dashed and dot-dashed lines are the theoretical cyclotron absorption and emission spectra of plasma in the magnetic field of the WD respectively. Thick solid lines are re-presenting the resulting fits to the continuum of the RX J1554.2+2721 in the high and low states (see the discussion in Sect. 4.3).

and c determine the relative contributions of the corresponding components. $F_{\rm em}$ and $F_{\rm abs}$ are functions of the magnetic field (B), the effective temperature of the underlying source (kT), the angle (Θ) between the magnetic field and the line of sight, and the dimensionless parameter $\Lambda = \omega_{\rm p} L/\omega_{\rm B} c$. Here $\omega_{\rm p}$ is the plasma frequency, $\omega_{\rm B}$ is the cyclotron frequency and L is the thickness of the plasma slab.

Low state spectrum: usually in similar cases one assumes a temperature (say 10 or 15 or 20 keV), also assumes a Θ (say 70 degrees), in order to find plausible parameters B and Λ, which will place synchrotron humps in the right places. Location of humps strongly depends on B and Λ parameters, while temperature (kT) and Θ parameter rather influence shape of the humps. Since in most of the cases there are many other contributing components, the fitting becomes limited by the "cross-correlation" of humps in the model with the observed spectra. Location of humps becomes crucial in determination of the magnetic field, which is the most relevant parameter.

However in RX J1554.2+2721 we somehow have a unique sort of low-state spectrum, where in order to achieve a good fit we do not need anything other than a secondary spectrum + $F_{\rm em}$. Thus we can fit $F_{\rm em}$ much more precisely than usually can be done. What we did was to do least-squares fitting along the spectrum with some initial parameters and floating all four of them and came up with a result, very nicely describing the observed data.

The hump at around Hβ is very distinct and it was easy to find the corresponding initial parameters, and afterwards refine them with least-square fitting. The contribution of the hot component $F_{\rm abs}$ in the low state spectrum was set to zero ($c = 0$). The calculated emission cyclotron spectrum is shown by a thin dashed-dotted line in Fig. 10. Its combination with a M4 v, secondary star spectrum (tiny dotted line) gives a resulting best fit to the low-state observed spectrum shown as the lower thick solid line in Fig. 10. The following parameters were inferred from the cyclotron emission model: $B = 31$ MG; $\Theta = 56°$; $kT = 14$ keV; $\Lambda = 6.6 \times 10^5$. Of course the shape of spectrum should change with orbital phase, thus the obtained parameters will vary too. That basically refers to Θ and Λ. Temperature is in the range in which one would expect to find in a polar, although it is higher than in HS 1023+3900. The M4 v secondary contribution is ∼50% of the total flux in the $R_{\rm c}$ filter and only ∼10% in the B band.

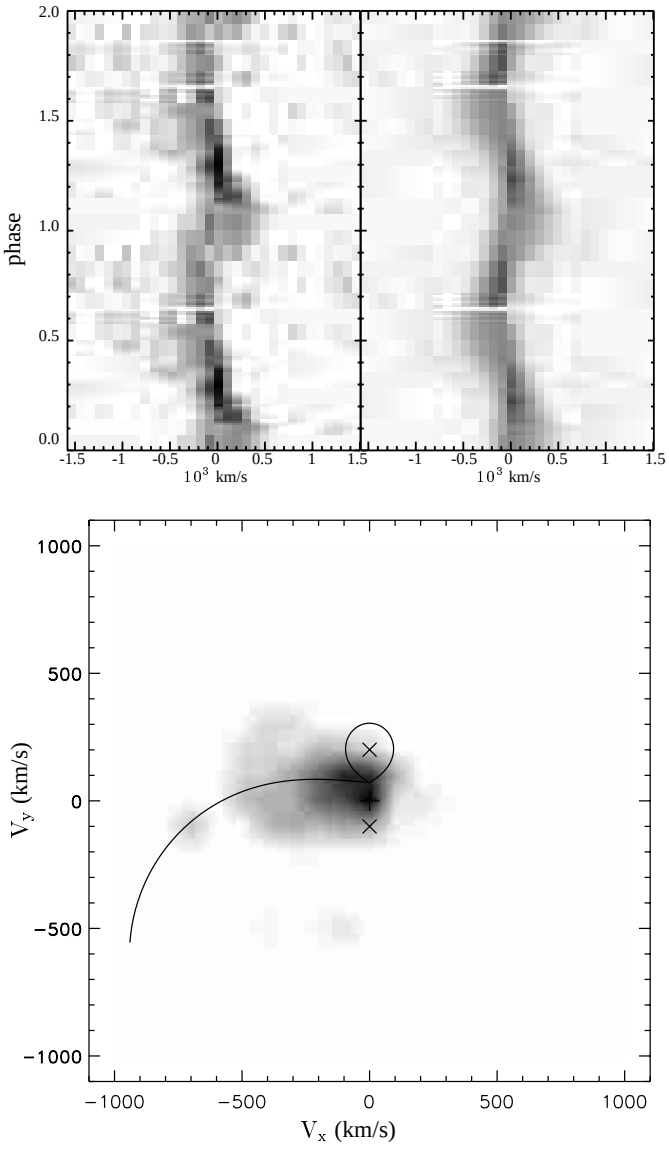

Fig. 11. Trailed, continuum-subtracted spectra around He II of RX J1554.2+2721 plotted in two cycles (upper panels). The doppler map of the He II emission line in velocity space (V_x, V_y) is given. A schematic overlay marks the Roche lobe of the secondary and the ballistic trajectory. The secondary star and gas-stream trajectory are plotted for arbitrary mass ratio $q = 0.5$ ($M_2 = 0.24\ M_\odot$) and inclination angle $i = 50°$.

The remaining deviation of the modelled spectrum from the observed one can be explain as the consequence of the deviation of the emission region geometry from the simple and homogeneous geometry of the Barrett & Chanmugam model, and/or the deviation of the radiation of the optical thin plasma in the magnetic field from thermal radiation.

High state spectrum: the examination of the spectra in the high state demonstrate that the hump at around $\lambda\,4800$ Å is still detected, although it is less pronounced. Thus, we believe that the spectrum in the high-state is composed of the same components as in the low state with the addition of a hot component which we identify as cyclotron emission from the optically thick portion of the plasma slab in the model. This component is responsible for the excess of flux in the near UV region. It is much steeper (in the wavelength range shortward of 4500 Å) than recombination emission, as can be seen in Fig. 9. Indeed, the addition of an absorption cyclotron component shown as a dashed line in Fig. 10, shows a good agreement between the composite spectrum and the observed one in the high state. The resulting fit to the high state spectrum is shown as another (upper) thick solid line in Fig. 10. Assuming that the high luminosity is due to a higher accretion rate, we suppose that an increase of matter in the accretion column may create favorable conditions for the appearance of an optically thick, absorption cyclotron spectrum. The parameters of the absorption cyclotron emission which we obtained from the fitting confirm this. With the magnetic field strength and angle remaining the same, the parameter $\Lambda = 40.6 \times 10^5$ shows a five-fold increase as compared to the emission spectrum from the optically thin layer in the optical low state. This increase most probably is conditioned by the increased density of the matter in the column. Meanwhile, the temperature of the optically thick matter better fits the observed flux at $kT = 18.5$ keV, but it may vary significantly without major impact on the final result. It is worth mentioning that in the high-state spectrum fits, both cyclotron components contribute, showing that we have optically thick and thin plasma at the same time. The temperature of optically thin emission-cyclotron radiation however remains at around 14 keV, as in the low state. But, the overall contribution of the optically thin emission is increased in comparison to the low state, which may be the result of an increase in the emitting area. The contribution of the corresponding components is estimated as follows: In the red part of the spectrum (R_c band) the contribution of emission-cyclotron emission rises to 60%, with the rest coming from the secondary star. In the B band the absorption cyclotron emission from the optically thick plasma contributes up to ∼40% of total flux, while the optically thin plasma is responsible for ∼55%, and the remaining ∼5% are coming from the secondary star. It is not excluded, however, that part of the emission in the near UV has a recombination origin. In that case the budget will be slightly different, of course. From our data it is difficult to estimate the relative contribution of recombination emission and optically thick cyclotron absorption. It is important, however, that recombination emission alone will not be enough to explain the blue/ultraviolet excess in the high state, and the scenario suggested above may be a reasonable alternative.

5. Doppler tomography

Doppler tomography (Marsh & Horne 1988) is a widely used method to extract further information on CVs from trailed spectra. In the case of magnetic CVs, particularly polars, Doppler tomography in most cases reveals a very

distinctive pattern: the compact spot appears at the location of the heated tip of the secondary star with a diffuse arm extending from the L_1 point almost perpendicular at first, then bending toward negative velocities (both V_x and V_y). It follows closely the calculated trajectory of free-falling matter from the Lagrangian point.

We used the code developed by Spruit (1998) to obtain a Doppler map of RX J1554.2+2721 using the maximum entropy method. The resulting Doppler map (or tomogram) of the He II emission line is displayed as a gray-scale image in Fig. 11. Also, trailed spectra of the He II line in phase space and its corresponding reconstructed counterpart are displayed in Fig. 11. The Roche lobe of the secondary calculated for a mass ratio $q = 0.5$ and an inclination angle $i = 50°$ is drawn on the map. These were selected from the values estimated from the light curve variations amplitude, due to the elliptically distortion of the secondary. Also shown is the accretion stream according to the above mentioned parameters. The resulting map is further good evidence in favor of the classification of RX J1554.2+2721 as a polar.

6. Conclusions

We have studied the new cataclysmic variable RX J1554.2+2721 discovered by ROSAT observations. The soft X-ray spectrum and strong X-ray variability immediately suggests a magnetic cataclysmic variable nature. The follow-up optical spectral and photometric observations provided additional support for this classification. The continuum spectrum shows direct evidence of the presence of a magnetic accreting WD in the system. These, combined with emission line profiles, RV curves and Doppler maps, and characteristic light curve undoubtedly supports the magnetic nature of RX J1554.2+2721.

We derived $P_{\rm orb} = 2\overset{\rm h}{.}753 = 165.2$ min for RX J1554.2+2721, placing it inside the period gap for CVs. This period is very close to (or even shorter than) the recently discovered HS 1023+3900 (Reimers 1999). The latter is considered unique, because it exhibits a pure cyclotron emission line spectrum. Reimers (1999) claims that the appearance of the spectrum is a result of an extremely low mass transfer rate, which in turn is supported by the evolutionary scenarios, according to which the mass transfer comes to a halt in the period gap and systems become undetached.

RX J1554.2+2721 is another system in this range of orbital periods showing a reduced accretion rate, and actually shows barely any in the low state. The switches between high and low states also demonstrate an unusual frequency, which may be the sign of a system at the verge of its accretion era. The continuous monitoring of this object may provide additional insights into the behavior of the CVs and particularly magnetic ones in the period gap.

We calculated the cyclotron spectra for RX J1554.2+2721 in the low and high states. Our main conclusions on the origin of optical radiation in the continuum are as follows:

1. RX J1554.2+2721 has a magnetic field strength of the WD of 3×10^7 gauss, and a postshock plasma temperature of 14 keV nicely consistent with the above-assumed 20 keV hard X-ray component.

2. In the low state we have a pure emission cyclotron spectrum from the optically thin cyclotron emitting source. In the high state we probably have a higher accretion rate, and we assume that an optically thick zone forms in the core of the accretion column. Therefore, the high state spectra can be described by enhanced low state emission plus additional radiation consisting of the combination of an optically thick cyclotron-absorption spectrum region and possibly recombination emission from reprocessed X-rays.

3. The remaining small deviations between the modelled and observed spectra of RX J1554.2+2721 can be explained as a consequence of the deviation of the emission region geometry from the simple geometry of the Barrett & Chanmugam model and/or the deviation of the radiation of the optical thin plasma in the magnetic field from a thermal model.

We estimate the mass and radius of the secondary star as $M_2 = 0.24\ M_\odot$ and $R_2 = 0.29\ R_\odot$ from the mass-period and radius-period relations of Echevarría (1983). The mass is consistent with the observed M4 V classification of the secondary and the assumption that it is not much different from a main-sequence star of corresponding temperature.

The mass ratio q and inclination angle i of the system were estimated from the amplitude of ellipsoidal variations of the secondary in the low state and independently confirmed and refined from Doppler tomography to be around 0.5 and 50°, respectively.

The distance to RX J1554.2+2721 also can be estimated from the intensity of the secondary in the spectra of RX J1554.2+2721 in the low and high states. The flux of the M4 V star at 5500 Å or in the V band, is 6×10^{-17} erg/cm^2/s/Å, corresponding to a brightness of $V = 19.45$ mag (for example, see Fukugita et al. 1995). A M4V star has $M_V = 12.95$ (for example G 165-8 in Henry et al. 1994). Assuming a maximum interstellar absorption in this direction of $A_V = 0.2$ mag (Dickey et al. 1990), we estimate a distance to this binary system of about 180–200 pc. Even if the high value of the distance estimates were correct, the correspondingly higher luminosity which we derive from the measured flux would still be lower than that of most magnetic CVs.

With a distance estimate available, we can also infer the accretion rate by assuming that the accretion luminosity is emitted mostly in X-rays. We apply equation 6.10 from Warner (1995) and estimate $\dot{M}$ using the bolometric luminosity from X-ray observation as $\dot{M} \sim 4 \times 10^{-12} (d/180)^2\ M_\odot\,{\rm yr}^{-1}$.

In this brief report we did not intent to derive all parameters of this very interesting new discovered polar. New observations are necessary to study this system in

more detail. Meanwhile, its existence seems to provide a good test bed for existing evolutionary models.

Acknowledgements. We are grateful to A. Pramsky and A. Ugryumov for help in SAO RAS 6m telescope observations. This work was supported in part by CONACYT project 25454-E and a DGAPA project.

References

Barrett, P., & Chanmugam, G. 1984, BAAS, 16, 943
Barrett, P., & Chanmugam, G. 1985, ApJ, 298, 743
Beuermann, K. 1998, in Perspective of High Energy Astronomy & Astrophysics. Proc. of Int. Coll. to commemorate the Golden Jubilee of TIFR, Tata Inst. of Fund. Research, India, Aug. 1996, 100
Chanmugam, G., & Dulk, G. A. 1981, ApJ, 244, 569
Cropper, M. 1990, SSRv, 54, 195
Deeming, T. J. 1975, Ap&SS, 36, 137
Dickey, J. M., & Lockman, F. J. 1990, ARA&A, 28, 215
Downes, R., Webbink, R. F., & Shara, M. M. 1997, PASP, 109, 345
Echevarría, J. 1983, Rev. Mex. Astron. Astrofis., 8, 109
Fischer, A., & Beuermann, K. 2001 [astro/ph 0105190]
Fukugita, M., Shimasaku, K., & Ichikawa, T. 1995, PASP, 107, 945
Henry, T. J., Kirkpatrick, J. D., & Simons, D. A. 1994, AJ, 108, 1437
Howell, S. B., Rappaport, S., & Politano, M. 1997, MNRAS, 287, 929
Howell, S. B., Ciardi, D. R., Dhillon, V. S., & Skidmore, W. 2000, ApJ, 530, 904
Jiang, X. J., Engels, D., Wei, J. Y., Tesch, F., & Hu, J. Y. 2000, A&A, 362, 263
King, A., & Cannizzo, J. 1998, ApJ, 499, 348
Li, J. K., Wu, K. W., & Wickramasinghe, D. T. 1994, MNRAS, 268, 61
Marsh, T. R., & Horne, K. 1988, MNRAS, 235, 269
Meggitt, S. M. A., & Wickramasinghe, D. T. 1984, MNRAS, 207, 1
Rappaport, S., Verbunt, F., & Joss, P. 1983, ApJ, 275, 713
Reimers, D., Hagen, H.-J., & Hopp, U. 1999, A&A, 343, 157
Ritter, H., & Kolb, U. 1995, in X-Ray Binaries, ed. W. H. G. Lewin, J. van Paradijs, & E. P. J. van den Heuvel (Cambridge: Cambridge Univ. Press), 578
Roberts, D. H., Lehar, J., & Dreher, J. W. 1987, AJ, 93, 968
Robinson, E. L. 1983, in Cataclysmic Variables and Related Objects, ed. M. Livio, & G. Shaviv (Dordrecht: Reidel), 1
Rousseau, Th., Fischer, A., Beuermann, K., & Woelk, U. 1996, A&A, 310, 526
Schwope, A. D., Mantel, K.-H., & Horne, K. 1997, A&A, 319, 894
Schmidt-Kaler, Th. 1982, Bull. Inf. Centre Donnes Stellaires, 23, 2
Spruit, H. C. 1998 [astro-ph/9806141]
Thorstensen, J. R., Fenton, W. H. 2001, private communication
Tovmassian, G. H., Szkody, P., Greiner, J., et al. 1999, Annapolis Workshop on Magnetic Cataclysmic Variables, ed. C. Hellier, & K. Muai, ASP Conf. Ser., 157, 133
Warner, B. 1995, Cataclysmic Variable Stars (Cambridge Univ. Press, Cambridge)
Wickramasinghe, D. T., & Wu, K. 1994, MNRAS, 266, L1
Woelk, U., & Beuermann, K. 1992, A&A, 256, 498
Zimmermann, H. U., Becker, W., Belloni, T., et al. 1994, MPE Rep., 257